Excitonic fine structure and binding energies of excitonic complexes in single InAs quantum dashes

P. Mrowiński,[1] M. Zieliński,[2] M. Świderski,[2] J. Misiewicz,[1] A. Somers,[3] J. P. Reithmaier,[4] S. Höfling,[3,5] and G. Sęk[1,*]

[1]*Laboratory for Optical Spectroscopy of Nanostructures, Division of Experimental Physics, Faculty of Fundamental Problems of Technology, Wrocław University of Science and Technology, Wrocław, Poland*

[2]*Institute of Physics, Faculty of Physics, Astronomy and Informatics, Nicolaus Copernicus University, Toruń, Poland*

[3]*Technische Physik & W. C. Röntgen-Center for Complex Material Systems, Universität Würzburg, Germany*

[4]*Institute of Nanostructure Technologies and Analytics (INA), CINSaT, University of Kassel, Kassel, Germany*

[5]*SUPA, School of Physics and Astronomy, University of St. Andrews, North Haugh, St. Andrews, United Kingdom*

(Received 6 July 2016; published 26 September 2016)

The fundamental electronic and optical properties of elongated InAs nanostructures embedded in quaternary InGaAlAs barrier are investigated by means of high-resolution optical spectroscopy and many-body atomistic tight-binding theory. These wire-like shaped, self-assembled nanostructures are known as quantum dashes and are typically formed during the molecular beam epitaxial growth on InP substrates. In this paper, we study properties of excitonic complexes confined in quantum dashes emitting in a broad spectral range from below 1.2 to 1.55 μm. We find peculiar trends for the biexciton and negative trion binding energies, with pronounced trion binding in smaller size quantum dashes. These experimental findings are then compared and qualitatively explained by atomistic theory. The theoretical analysis shows a fundamental role of correlation effects for the absolute values of excitonic binding energies. Eventually, we determine the bright exciton fine structure splitting (FSS), where both the experiment and theory predict a broad distribution of the splitting varying from below 50 to almost 180 μeV. We identify several key factors determining the FSS values in such nanostructures, including quantum dash size variation and composition fluctuations.

DOI: 10.1103/PhysRevB.94.115434

I. INTRODUCTION

Self-assembled InAs quantum dashes (QDashes) are rather unconventional semiconductor nanostructures with characteristic large in-plane elongation. The potential of QDashes for applications has been demonstrated in various ways, including the utilization as a gain medium for lasers and amplifiers [1,2] but also as single photon emitters operated both on charged and neutral excitons [3,4]. Of special importance and specific for these structures is that they are possible to systematically reduce the exciton fine structure splitting (FSS) below the natural linewidth of emission, which makes the QDashes prospective as a source of polarization entangled photon pairs from biexciton-exciton cascade [5]. Such an FSS control seems to be typical for any of QDashes in this material system due to their intrinsic exciton spin properties [5], which has not been demonstrated to that extent for any other quantum-dotlike nanostructures, especially in InP-based nanostructures emitting at telecommunication wavelengths. Examples of FSS external control have been reported for more symmetric quantum dots of the InAs-GaAs material system, e.g., by applying electric field to low-strained InAs/InGaAs quantum dots emitting around 1260 nm [6] or by magnetic field applied to InAs/GaAs quantum dots emitting below 900 nm [7]. Moreover, QDash exciton bright states exhibit a significant polarization anisotropy of emission [8–10], which together with further enhancement by a simple postgrowth patterning of dielectric medium can offer an efficient source of linearly polarized single photons [8,10,11] that seems to also be quite a unique and application-relevant property of the dashes. All of these overlap with the second or third telecommunication data transmission windows [12–14] and thus allow considering the QDashes for realization of selected issues in quantum information processing [15–17] and nanophotonics [7,18–21].

QDashes are formed in a common self-assembly of molecular beam epitaxy, and if they can be used as-grown their fabrication is less challenging than nanostructures obtained by more advanced treatment such as site-controlled methodology [22–24] or strain compensation as for GaAs-based quantum dots for tuning to telecom spectral range [25,26], which can hardly reach the 1.55 μm range. In spite of the aforementioned technological and device-related perspectives, the fundamental electronic and optical properties of QDashes are still barely known. For such strongly in-plane elongated nanostructures based on InP, there is no systematic investigation of the influence of morphology and size (energy of emission) on the binding energies of excitonic complexes or the FSS, or, in particular, how significantly the asymmetric potential of the dashes makes them different from the more symmetric InAs-InP-based nanostructures [27–32]. Such quasi-0D (quasi-zero-dimensional) structures can offer unique properties hardly accessible in other systems but can also enlighten the understanding of the intermediate regime between strong and weak confinement. Furthermore, it is interesting to learn which factors influence the direct Coulomb interactions, correlations, and exchange that affect the binding energies or the exciton fine structure. This paper should fill this gap, leading to a better control of these parameters for the next generation of the application-relevant nanostructures using the InP-based material system.

The role of morphological details, such as size and shape and composition profile, on the electronic states (and confinement potential) has been addressed both experimentally and theoretically on numerous kinds of III-V material systems [33–38], including also InAs on InP [28,30] but for only

*grzegorz.sek@pwr.edu.pl

slightly asymmetric structures. For example, the importance of correlations, when the size of the nanostructure increases, has been deduced by observing biexciton binding energy increase due to smaller separation between excited hole states [34]. Other studies have shown also a high sensitivity to relative size and position of electrons' and holes' wave functions [39].

It is well known that the exciton FSS induced by the exchange interaction is very sensitive to the symmetry of the confinement potential; however, the dependence is not always straightforward and differs from system to system due to various factors affecting the confinement potential itself or the electron-hole separation. It has been shown, for instance, that even ideal cylindrical symmetry of a nanostructure is not sufficient for obtaining the zero-FSS value due to built-in intrinsic contribution related to the crystal lattice asymmetry [40]. The degeneracy itself is lifted by several μeV, while in the envelope function theoretical treatment it is irrelevant for symmetric structures. Even though this is the case, most of the self-assembled quantum dots are far from the cylindrical shape in the plane, leading very often to FSS on the order of 100 μeV [41,42]. Such high values that have been observed experimentally are often missed by theoretical predictions made by $k \cdot p$ [35] or the empirical pseudopotential method [43]. So far, some challenges have been successfully solved by the atomistic tight-binding approach [42,44], which may also be employed for other nontrivial nanostructures. Using atomistic theoretical calculations for deriving excitonic recombination energies that are available experimentally by means of optical measurements, the assessment to the basic structural information has been performed [33,45]. Additionally, for highly disordered structures, the lattice randomness methodology has been examined in order to explain variations in the ordering of the emission spectra within a quantum dot ensemble [46].

Hereby, single QDashes were investigated both experimentally, using microphotoluminescence, and theoretically, by using the atomistic tight-binding theory combined with the configuration interaction (CI) method. Excitonic complexes have been identified in a broad spectral range of emission from 0.8 to above 1.0 eV (1.2–1.55 μm), and binding energies of biexciton, charged exciton (trion), and the exciton FSS have been studied. By introducing an elongated geometry with a wedge-shaped cross-section and intermixing of materials, Coulomb integrals and correlation corrections were analyzed as a function of the exciton emission energy. A realistic strongly asymmetric in-plane shape is assumed in order to verify the calculated FSS dependence with respect to the experimental data.

II. EXPERIMENTAL

The investigated structures were grown by a gas-source EIKO molecular-beam epitaxy system using S-doped InP(001) substrates. A self-assembled InAs layer is deposited at 470°C on an InGaAlAs barrier lattice matched to InP preceded by an InP buffer layer. The same quaternary barrier is used to cover the QDashes, and then the sample is capped with 10 nm thick InP. The surface density of QDashes can reach $5 \times 10^{10}\text{cm}^{-2}$. Significant inhomogeneity of the ensemble combined with etched submicrometer mesa structures allow for probing a relatively small number of QDashes at once and for the observation of single, sharp, and well separated

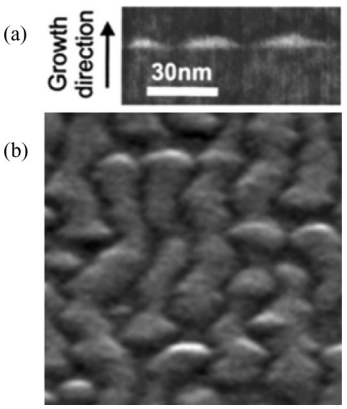

FIG. 1. (a) The STEM micrograph of cross-sectional sizes of single QDashes (after Ref. [12]) showing a triangular geometry and (b) the SEM image of the uncapped QDash layer.

emission lines. The typical triangular-shaped cross-section of QDashes has been verified by scanning transmission electron microscopy (STEM) [Fig. 1(a)], which also showed that increasing the amount of deposited InAs material enlarges proportionally both the height (approximately 2–4 nm) and width (approximately 10–20 nm) of the nanostructures, leading to a change in the emission wavelength [2,12,13,47]. Although it is difficult to precisely determine the length scaling according to a scanning electron microscope (SEM) image of uncapped QDash layers [Fig. 1(b)], the nominal elongation of more than 50 nm is observed. Due to the small lattice mismatch of $\sim$ 3–4% [48], the atom's surface diffusion coefficient anisotropy is more pronounced, and then the epitaxially formed nanostructures are significantly elongated in one of the distinguished crystallographic in-plane directions (preferentially along [1–10]) [25,49].

For single dash spectroscopy, a microphotoluminescence setup was used, equipped with a 1-m focal length monochromator, an InGaAs detector array, and a long working distance microscope objective with a numerical aperture of 0.4 to focus the excitation beam and to collect the emission. The spectral resolution is estimated to be about 20 μeV for these measurements. Polarization-resolved analysis is performed using a half-wave plate in front of horizontally aligned linear polarizer, and the optical spectra for orthogonally polarized spectral lines can be resolved down to $\sim$5 μeV. The sample is excited nonresonantly under normal incidence by a continuous-wave laser diode emitting at 660 nm, which is focused on the sample surface to approximately a 2-μm-sized spot. The size of etched mesas is even smaller in order to further limit the number of probed nanostructures. The photoluminescence signal is collected backward and transmitted through the half-wave plate, a dichroic mirror and linear polarizer aligned for maximum efficiency of the diffraction grating. Such order provides the independence of the measured intensities of the setup polarization characteristics.

III. RESULTS AND DISCUSSION

A. Luminescence

Photoluminescence taken at 10 K from the large ensemble of InAs/InGaAlAs/InP QDashes of three samples differing by

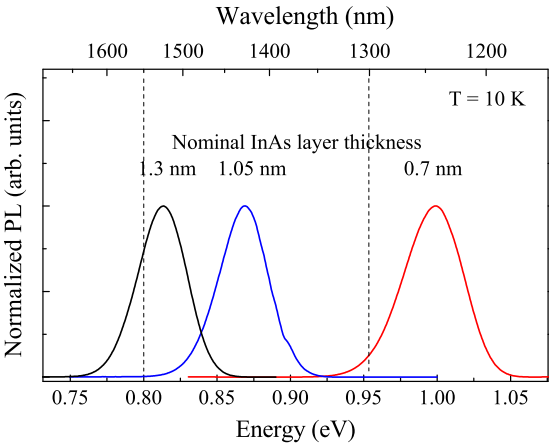

FIG. 2. Photoluminescence emission from quantum dash ensemble for different nominal InAs layer thicknesses overlapping with the second (1300 nm) and third (1550 nm) telecommunication low loss windows.

the nominal amount of deposited InAs is presented in Fig. 2, which shows the available spectral range for detection and analysis of single excitonic transitions. The tuning is in fact realized by mainly affecting the cross-sectional size [12,50], and the resulting distribution of the emission shows the overlap with 1.3 and 1.55 μm, which is relevant from the application point of view in secure communication technologies.

An extracted microphotoluminescence spectrum of a single QDash is shown in Fig. 3(a). It is taken on a structured mesa of $400 \times 400\,\mathrm{nm}^2$, which is sufficient for the observation of well separated optical transitions [4,14,51]. Figure 3(a) shows three spectral features around 990 meV (∼1260 nm) detected for four different excitation power conditions. The intensity dependence versus the excitation power is plotted in the inset of Fig. 3(a) in order to verify the slope of this dependence in the range of low excitation, which is close to linear for the lines at 994.6 meV and 989.1 meV. The middle transition is not visible at low excitation, and after increasing the excitation, a superlinear increase is observed. The same spectra are shown in Fig. 3(b) for two perpendicular linear polarizations aligned with respect to [110] and [1–10] directions taken from full-rotation polarization series. A splitting on the order of

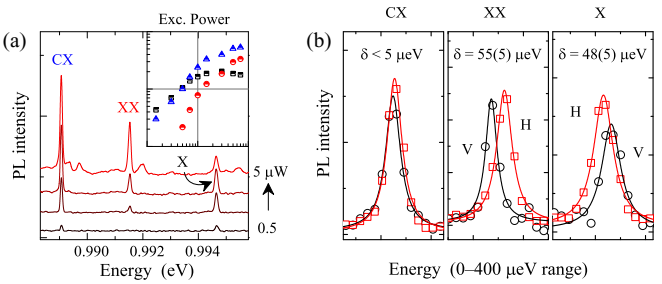

FIG. 3. (a) Microphotoluminescence spectra for various excitation powers from 0.5 to 5 μW. The inset shows the intensity dependence with a slope variation depending on the spectral feature. (b) Polarization resolved spectra showing fine structure splitting indicating exciton and biexciton emission and no splitting for charged exciton.

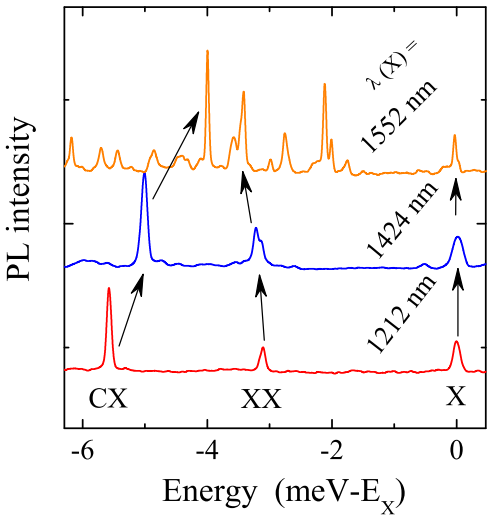

FIG. 4. Excitonic complexes for different emission wavelengths showing alike spectroscopic pattern for biexciton and trion transitions.

50 μeV for higher energy transitions and a lack of splitting for the lowest energy line is observed. A vanishing splitting is expected for a charged exciton emission due to the canceled exchange interactions in the case of a single particle residual spin of electron or hole; the transition in the middle is assigned to a biexciton (XX) due to superlinear increase and the high-energy line to exciton (X) by its noticeable FSS. In this scheme, the spectral energy difference between exciton and biexciton of −3.1 meV and between the exciton and charged exciton of −5.7 meV can be determined, indicating the binding states for both. No signature of any unbound state on the higher energy side of the spectrum has been identified.

Figure 4 shows three other examples of excitonic complexes at various wavelengths of emission taken on the structured mesas. The origin of the lines has been determined in the same way as above, confirming the neutral exciton, the biexciton, and one bound trion. The energetic difference changes smoothly for the cases emitting at around 1212 nm, 1424 nm, and 1552 nm. Such spectra reveal a specific spectroscopic pattern for optically active single InAs QDashes, as also confirmed by the measurements of the second-order cross-correlation function presented elsewhere [3,4]. Although for the case emitting close to 1552 nm, the spectral density is relatively high; the other optical transitions have been verified as not correlated with identified excitonic complexes from a single QDash by the same methodology. This lack of correlation with other spectral features suggests that an oppositely charged trion might be unattainable experimentally in this system.

B. Binding energies and FSS

The spectroscopic data have been collected for more than 50 single InAs QDashes in a way described in the previous section. The spectral range is limited to about 0.8 eV on the lower energy side by a detection efficiency decrease of the InGaAs detector used in our experiments, whereas the maximal energy is 1.05 eV and corresponds to the smallest

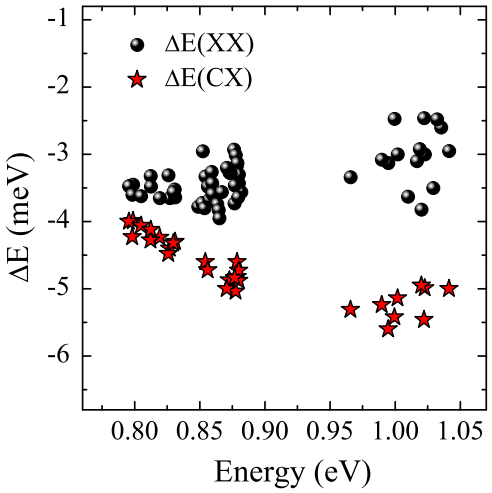

FIG. 5. Binding energy of biexciton (circle) and charged exciton (star) state determined for ca. 50 single QDashes in dependence of exciton emission energy.

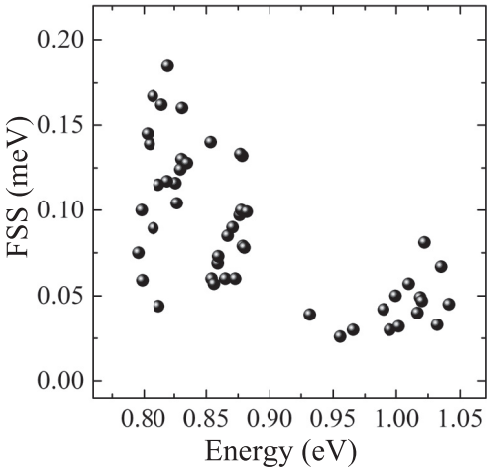

FIG. 6. Exciton fine structure splitting averaged from biexciton and exciton transition in emission energy dependence.

available QDashes. In Fig. 5, the determined binding energies of biexciton and trion in function of emission energy of exciton from the same QDash are shown. According to the definition of binding energy $\Delta E(X^*) = E_{X^*} - E_X$, which is related to photon energies emitted by an excitonic complex X^* and exciton X given by E_{X^*} and E_X, respectively, the value of $\Delta E(X^*)$ implies a bound (unbound) state when it is negative (positive), and E_{X^*} is lower (higher) than E_X. One needs to be careful with such a notation (which, however, reflects better the physical situation in our opinion) when comparing to results of other papers where oppositely defined binding energies can also be used. As seen in Fig. 5, all binding energies determined here remain on the negative side of the energy scale; therefore, sometimes absolute values are referred to when necessary. The size dependence in Fig. 5 is very smooth for the biexciton, and its magnitude decreases slightly with increasing energy of emission (binding energy decreases). The distribution appears to be narrower on the lower energy side where the binding energy is equal to about −3.5 meV. It gets more spread out when going to higher exciton energies and can reach values from −2.5 to −4 meV. This might be related to the intermixing effect with the InGaAlAs barrier, where smaller nanostructures may be more sensitive to small fluctuations of shape and composition (see the theoretical analysis in the next section). In the case of the charged exciton, the distribution broadening effect is not pronounced. However, the emission energy dependence for the charged exciton shows a more evident increase of the binding energy with the emission energy (binding energy varies from −4 meV to −5.8 meV). The gap in the data of Fig. 5 in the energy range between 0.9 and 0.95 eV is related mainly to the experimental difficulties in dealing with a strong water-vapor-related absorption overlapping with relatively weak optical transitions.

Figure 6 shows the FSS of the bright exciton determined by the average of values obtained from the respective biexciton and exciton emissions polarized along [1–10] and [110] directions. The largest splitting amounts to approximately 190 μeV, which is, however, not the largest reported in spite of extraordinary asymmetry of the investigated system [28,31]. What is noticed is that there is no clear dependence on energy of emission; instead a vast distribution of the FSS from below 50 μeV to above 150 μeV is observed for the 0.8–0.9 eV energy range. Based on this observation, it can be concluded that the confinement potential is very random from QDash to QDash, possibly partly due to previously predicted and verified localized centers that might exist in the optically active structures within such nanostructure exhibiting irregularities in morphology [9]. A much more regular behavior is seen in the emission range around 1 eV where the FSS is typically between 40–60 μeV with few exceptions above this range. The conclusion is that the potential anisotropy related to the typical elongation of QDashes must be relevant, leading to a stronger influence of the exchange interaction, while smaller splittings are possible due to geometrical (or compositional) fluctuations in the plane of some dashes, which might confine excitons in a smaller and less anisotropic volume [9].

C. Theoretical considerations

The InAs QDashes as highly elongated wedges with triangular shaped cross-sections are modeled according to available morphological data (schematics shown in the inset of Fig. 7). A family of systems with heights varying from 1.8 to 4.2 nm (i.e., 6 to 14 monolayers) is studied. To simulate the realistic tendencies in which the characteristic sizes scale linearly [12], both the height to base width and the length to base width ratios were kept constant and equal to 4. Hence, the base width varies from 7.2 to 17 nm and the length from 28.8 to 68 nm. Once the geometry of the system is established, the equilibrium atomic positions using the valence force field (VFF) model of Keating [52–54] are calculated.

In these calculations, QDashes using two different compositions, the first being pure InAs, are modeled. However, the realistic nanostructures are always a subject of alloying and lattice randomness. Therefore, in the second approach, a system with the barrier material mixed into the QDash is also studied. In particular, an intermixed case is considered, where the

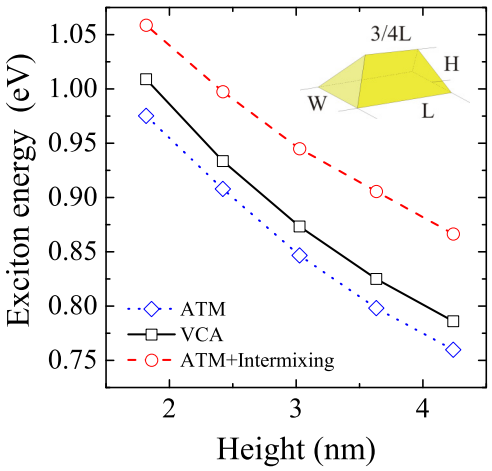

FIG. 7. Exciton ground state energy calculated using different atomistic approaches as a function of quantum dash size (H – Height, $W = 4 \times H, L = 4 \times W$).

pure InAs QDash composition was replaced with (uniformly distributed) $In_{0.9}Ga_{0.05}Al_{0.05}As$ alloy [55]. Additionally, the QDash and the surrounding InGaAlAs barrier were modeled using two distinct methods as well. In the first approach, virtual crystal approximation (VCA) is used, where the VFF parameters are taken as a weighted average of the barrier material (GaAs, AlAs, InAs) parameters. In the second fully atomistic approach, the surrounding matrix (and the dash in the alloyed case) is treated as a set of individual atoms in random positions. The uniform composition profile of the desired alloy ($In_{0.528}Ga_{0.234}Al_{0.238}As$) is considered. It is also noted that in several cases, calculations for InAs QDashes embedded in pure InP barrier were performed (for comparison purposes).

Once the atomic positions are found, the single particle states are calculated using an atomistic $sp^3d^5s^*$ [44,54,56,57] tight-binding model that accounts for d orbitals and the spin-orbit interaction and is capable of treating quaternary alloys such as InGaAlAs. Similarly, in order to calculate strain, the electronic structure calculation was performed using either the VCA or fully atomistic approach. In the VCA method, alloys were treated by defining tight-binding parameters as weighted averages of materials constituting the system. In this case, the valence band offset [48,57] between InAs QDash and the mixed $In_{0.528}Ga_{0.234}Al_{0.238}As$ matrix was set to 0.226 eV (based on the band offset values from Ref. [48]). In the fully atomistic treatment, arsenic atoms in the quaternary alloy (as well as arsenic atoms on the interfaces) have their on-site parameters calculated as an average of the nearest neighbors. Finally, the single particle calculation is followed by the many-body CI [54] calculation that produces the energy and optical spectra of excitons and excitonic complexes. In the CI, all the possible determinants constructed from the 12 lowest-energy electron and 12 lowest-energy hole states (including spin) were included. Finally, the optical spectra are found by calculating the oscillator strength for optical transition due to the recombination of one electron-hole pair in a given exciton state using Fermi's golden rule [54].

Figure 7 shows single exciton ground state energy as a function of the QDash height calculated using different atomistic approaches: VCA, fully atomistic model (ATM), and fully atomistic approach with the alloyed QDash composition (ATM+Intermixing). As discussed earlier, the change of QDash height corresponds to the change of all dimensions of QDash, i.e., base and length as well. Therefore, exciton energy shows a pronounced decrease from over 1.0 eV to below 0.8 eV, with the increasing dimensions due to the decrease of a quantum confinement. Similar results have been observed in the experiment, as shown earlier. In general, the difference between the VCA and ATM approaches is on the order of 25 meV, with ATM results systematically lower than the VCA ones; it is speculated that this is probably due to more efficient strain relaxation in the ATM model. On the other hand, energies given by the ATM model with the intermixing are typically larger by ~0.1 eV from ATM (without intermixing). This effect is an expected consequence of incorporation of the wide-band gap barrier material into the QDash structure.

In order to study the energy spectra of QDashes, the definition of the excitonic complex binding energy is used, which for a given complex is calculated with respect to the energy of the single (neutral) exciton as follows [46,58,59]:

$$\begin{aligned}\Delta E_{\mathrm{CI}}(XX) &\equiv E_{XX} - E_X = J_{\mathrm{ee}} + J_{\mathrm{hh}} - 2J_{\mathrm{eh}} - \Delta \mathrm{E}_{\mathrm{corr}}(XX)\\ &= \Delta E_{\mathrm{HF}}(XX) - \Delta E_{\mathrm{corr}}(XX)\\ \Delta E_{\mathrm{CI}}(X^-) &\equiv E_{X^-} - E_X = J_{\mathrm{hh}} - J_{\mathrm{eh}} - \Delta \mathrm{E}_{\mathrm{corr}}(X^-)\\ &= \Delta E_{\mathrm{HF}}(X^-) - \Delta E_{\mathrm{corr}}(X^-).\end{aligned}$$

Herein, the CI index denotes values calculated by the full CI approximation; as used in this paper, E_{XX}, E_X-, and E_X are biexciton, charged exciton, and exciton recombination energies. The binding energies were further divided into two contributions. The spirit of the Hartree-Fock (HF) (single configuration) approximation is seen in the first part of equation (HF) with an estimation of the binding energy. The second part of equation (correlations [corr]) is the correction due to correlations that account for effects of configuration mixing. Whereas inaccurate, the HF approach allows for simplified analysis, and it utilizes several Coulomb matrix elements only. These are namely $J_{\mathrm{ee}}, J_{\mathrm{eh}}$, and J_{hh}, which are correspondingly electron-electron, electron-hole, and hole-hole Coulomb integrals calculated for the electron (e) and hole (h) in their ground states.

Figure 8 shows these integrals calculated using three different approaches for the atomistic calculations and for several QDashes of different shapes. It is observed that the magnitude of these integrals grows with increasing values of the exciton energy. This is a hallmark of quantum confinement, which is stronger for smaller QDashes with higher excitonic energy. The stronger confinement results in stronger wave-function overlap leading to a more pronounced electron-electron, electron-hole, and hole-hole interactions. Moreover, when going beyond the VCA model, one observes fluctuations on top of clear monotonic trends: These are related to the lattice randomness. In the ATM case, there are composition fluctuations in the barrier region only, where only tails of QDash wave functions are localized. On the contrary, in the ATM+Intermixing case, both the barrier and the QDash are subject to lattice randomness, and hence there are more pronounced fluctuations of the Coulomb integrals values.

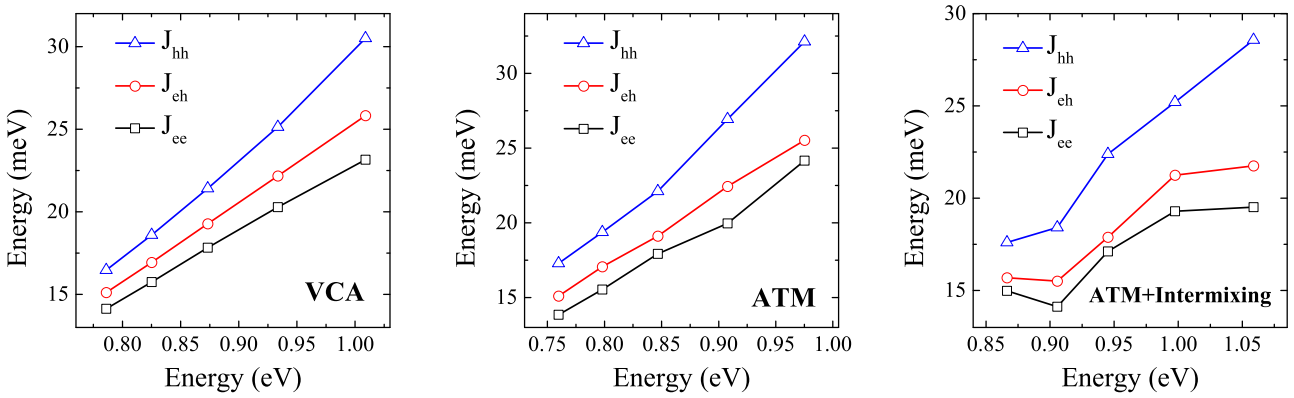

FIG. 8. Electron-electron (J_{ee}), electron-hole (J_{eh}), and hole-hole (J_{hh}) Coulomb integrals for electron and hole occupying their ground states calculated for several QDashes of different energy and using different atomistic approaches.

Apart from fluctuations, there is a common characteristic for all three models: the hole-hole repulsion grows faster with the increasing confinement than the two other integrals. The relatively strong repulsion between holes could be understood in terms of their higher effective mass leading to stronger confinement than that of electrons and thus larger susceptibility to change in nanostructure dimensions. Additionally, the hole states are formed predominantly from the p-type atomic orbitals of highly-directional character and as such are affected not only by the hydrostatic strain but also by the (highly anisotropic) biaxial strain. On the other hand, the electrons are constituted by s-type atomic orbitals—they reveal no angular dependence and thus are affected by hydrostatic component of strain only. Therefore, the hole states should, in principle, be more susceptible to QDash anisotropy resulting from highly-elongated geometry. This anisotropy is particularly strong for smaller QDashes, where hole states are affected by strong lateral confinement in the [110] direction and weak confinement in the [1–10] direction. The increased hole-hole repulsion has further a pronounced effect on the excitonic spectra.

Next, the energy spectra of excitonic complexes for variety of modeled structure geometries are considered. Calculations indicate that the positively charge exciton (X^+) is strongly unbound, i.e., its energy is several meV larger than the X energy. Therefore, our theoretical results suggest that the CX complex observed experimentally should be identified as X^-. Hence, in the following, attention is focused on X, X^-, and XX complexes. Figure 9 shows the biexciton and the negatively charged exciton ground state emission energies calculated with respect to the ground state energy of the single exciton and presented as a function of the exciton energy. Importantly, all three models show characteristic trends with a pronounced X^- binding energy dependence on the exciton energy (and thus effectively on QDash size), whereas the biexciton binding energy dependence remains relatively flat. Our calculations underestimate the absolute magnitude of excitonic complexes binding energies by about 1 meV when compared to the experimental data, most likely due to the difference between shape and composition assumed in theory and those of the actual QDashes, which can however be hardly determined with any better precision. Additionally, in our CI approach, as calculated in a limited basis (due to computational limitation), a further increase of the basis would likely lower the excitonic complexes binding energies. Moreover, any other more subtle effects as, e.g., coupling to phonons, which can also affect the binding energies [60], have not been included. Nevertheless, our theoretical results reproduce well the characteristics as seen in the experiment.

Figure 10 shows the biexciton and the negatively charged exciton binding energies in function of the ground state energy of the neutral exciton, calculated by using both the VCA at

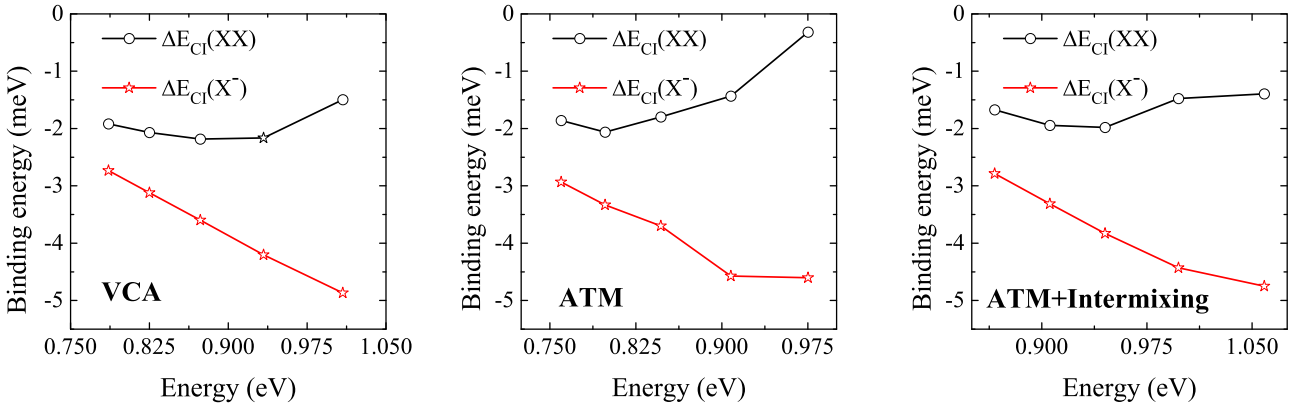

FIG. 9. Binding energies of biexciton (circles) and charged exciton (stars) calculated using a configuration interaction model and different atomistic approaches (see the text) as a function of exciton emission energy.

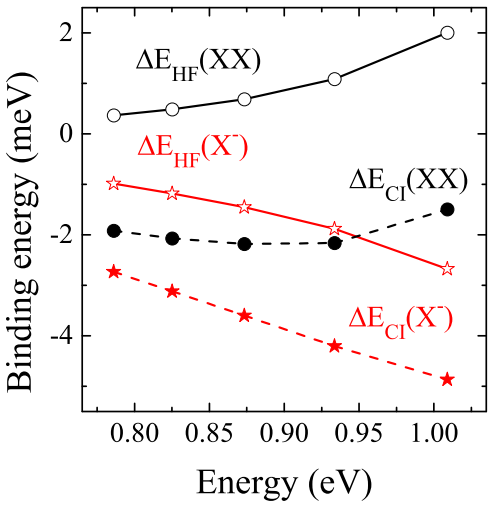

FIG. 10. Negatively charged exciton $\Delta E(X^-)$ and the biexciton $\Delta E(XX)$ binding energies in Hartree-Fock (HF) and configuration interaction (CI) pictures, calculated using VCA (see the text).

the level of HF approximation and the CI model. The HF model predicts in this case an unbound biexciton (i.e., having positive binding energy). As the hole-hole repulsion increases with the enhancement of the confinement, the (positive) binding energy increases as well. Thus, at the level of HF approximation, the biexciton remains unbound in all cases, with the large positive binding energy growing with X energy and reaching up to 2 meV for the smallest considered system. With correlations accounted for by the CI method, the XX binding energies are considerably shifted down in the energy in the direction to negative values (correction varying from -2 to -4 meV) and reveal quite a flat trend in the X energy, opposed to that predicted by the HF method only. In other words, QDashes are highly correlated systems, and thus the magnitude of correction due to correlations exceeds the contribution obtained by the rather simplified HF approximation.

Correlations have also a significant effect on the negatively charged exciton spectra, changing their binding energy by approximately -2 meV. Importantly, however, the overall trend of the X^- binding energy is quantitatively well reproduced already at the level of HF approximation: The X^- binding energy grows with the X ground state energy. At the level of HF approximation, this binding energy is given simply as a difference of electron-electron repulsion and electron-hole attraction (J_{ee}-J_{eh}). As shown earlier in Fig. 8, the electron-hole J_{eh} attraction grows faster with the confinement than electron-electron repulsion and hence results in the growth of X^- binding energy with increasing confinement.

Finally, the bright exciton FSS [61] is considered, as shown in Fig. 11. Our theoretical results demonstrate that the FSS decreases with increasing X emission energy. In other words, the FSS increases with the overall QDash size. Such dependence of the anisotropic exchange interaction [61] is opposite to that of the direct Coulomb interactions discussed above. The Coulomb direct terms could have been understood in terms of increased wave-function overlap in a smaller, more confined nanostructure, whereas this apparently does not apply to the FSS. Traditionally, the FSS is associated with the nanostructure shape elongation [35,61]. This is, however, not exactly a case here, since in our simulation a fixed lateral aspect ratio (4:1) is used. Recent theoretical progress [42,62–64] in the understanding of the excitonic fine structure points at the anisotropy of the overall (lattice+shape) confinement potential rather than shape elongation only. Thus, apart from the base elongation, the QDash anisotropy comes from the presence of atomic interfaces at the top four facets of a QDash: the larger (longer and taller) the QDash, the larger the area of these facets and hence the more pronounced role of anisotropy related to atomic interfaces, resulting in the increased FSS.

The calculated reduction of the FSS with the X emission energy is in relatively good agreement with the experiment (Fig. 6): The FSS is reduced approximately by a factor of four when going from 0.8 eV to 1 eV of the exciton emission energy. It is noted, however, that there is yet another important factor affecting the FSS: intermixing and its related lattice randomness. From one point of view, intermixing increases the X emission energy, as discussed earlier; on the other hand, it also smears out the potential anisotropy [42,65]. In effect, already at $x = 0.05$ of barrier material intermixed into the QDash region [Fig. 11(c); ATM+Intermixing], the FSS is reduced by about 20–30 μeV, as compared to the case without intermixing (ATM). High intermixing level $x \geqslant 0.10$

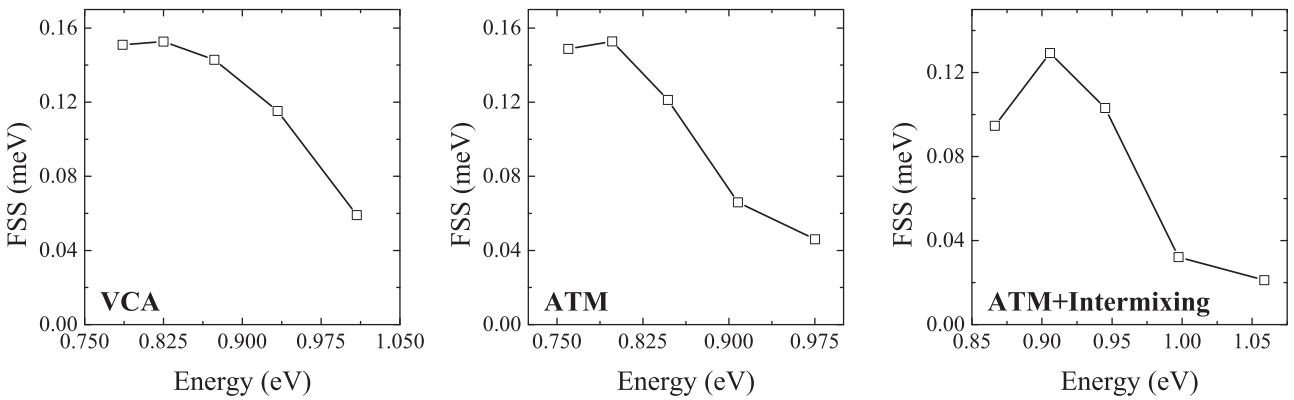

FIG. 11. Exciton fine structure splitting calculated using different atomistic approaches (see the text) as a function of exciton emission energy.

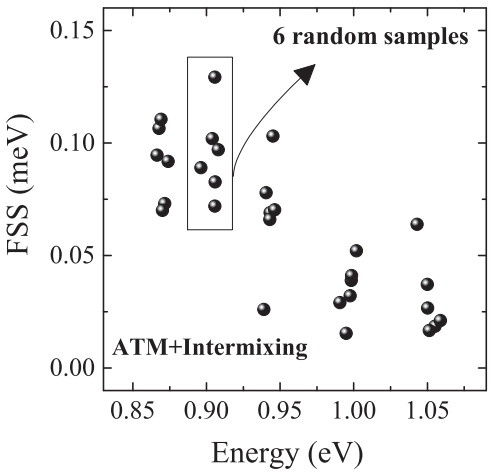

FIG. 12. Exciton fine structure splitting calculated to illustrate the role of lattice randomness. These results were obtained by putting together six random realizations (samples) for each quantum dash size (five different sizes) considered in the paper, giving a total of 30 systems. Each sample corresponds to different local atomic arrangements, whereas the average composition remains constant in all samples [46]. Calculations were performed using the ATM+Intermixing model, where $In_{0.9}Ga_{0.05}Al_{0.05}As$ QDash was embedded in the $In_{0.528}Ga_{0.234}Al_{0.238}As$ barrier.

corresponding to X emission energy ∼1.1–1.2eV, unobserved in the experiment, has additionally been calculated. At this level of the intermixing, the FSS is pushed down well below 40 μeV and strongly varies from QDash to QDash. Thus, apart from the FSS reduction, the intermixing introduces significant fluctuations of the FSS value [42]. The role of lattice randomness is particularly visible in Fig. 12. In this figure, the exciton FSS was obtained by running calculations for six random realizations (samples) for each QDash size considered in the paper. Since five different QDash sizes are considered, this gives a total of 30 systems. Each sample corresponds to different local atomic arrangements, whereas the average composition remains constant in all samples (please note, in particular, Fig. 1 of Ref. [46]). Calculations were performed using the ATM+Intermixing model, where the $In_{0.9}Ga_{0.05}Al_{0.05}As$ QDash was embedded in the $In_{0.528}Ga_{0.234}Al_{0.238}As$ barrier. As shown in Fig. 12, the intermixing leads to a broad distribution of FSS values on top of general size-dependent trends. Despite the relatively simple, uniform composition profile assumed in our calculations, the predicted FSS values are in qualitative agreement with the experimental results (Fig. 6). It is concluded that the atomistic calculations suggest that lattice randomness, as well as QDash shape and size variations, are responsible for the broad distribution of FSS values observed in the experiment.

IV. CONCLUSIONS

In this paper, single QDash nanostructures emitting in a broad spectral range from 0.8 eV to above 1 eV made of InAs/InGaAlAs on InP were examined both experimentally and theoretically. A satisfactory agreement between microphotoluminescence spectra and calculated energies by atomistic tight-binding approach using the CI method was obtained. The data concerns the binding energy dependence of both the biexciton and the negatively charged exciton, as well as the exciton FSS. Our results show that the electronic structure of this system is strongly influenced by Coulomb correlations, which are reflected in the negative biexciton binding energy of about −3.5 meV with rather smooth energy dependence and even more bound negative trion of binding energy in range of −4.5 to −5.5 meV. There is no evidence of the positively charged trion in the experiment due to a possible high concentration of excess carriers. By calculated energies of excitonic complexes, an atypical increase of correlations for smaller QDashes, which is related to the strain field that affects the charge spacings due to size change, was observed. The exciton FSS is experimentally largely distributed, suggesting strong impact of the structural details. However, by performing calculations for a fixed lateral aspect ratio of 4, it is identified that increasing proportionally the nanostructure dimensions causes higher energy splittings reaching about 150 μeV, which is comparable to the measured values in the upper limit. By introducing the intermixing to the system, smaller FSS was obtained, suggesting that atomistic rearrangement between the QDash and the barrier structure might be a reason of the broad data distribution at a given spectral range.

ACKNOWLEDGMENTS

We would like to thank Paweł Machnikowski from the Division of Theoretical Physics, Wroclaw University of Science and Technology, for critical reading of the manuscript and his valuable comments. The work has been supported by the National Science Centre of Poland within Grant No. 2011/02/A/ST3/00152 (Maestro) acknowledged by P.M., J.M., and G.S. and Grant No. 2015/18/E/ST3/005 (Sonata Bis) acknowledged by M.Z. The experiments have partially been performed within the Wroclaw University of Science and Technology laboratory infrastructure financed by the Polish Ministry of Science and Higher Education Grant No. 6167/IA/119/2012.

[1] J. P. Reithmaier, A. Somers, S. Deubert, R. Schwertberger, W. Kaiser, A. Forchel, M. Calligaro, P. Resneau, O. Parillaud, S. Bansropun, M. Krakowski, R. Alizon, D. Hadass, A. Bilenca, H. Dery, V. Mikhelashvili, G. Eisenstein, M. Gioannini, I. Montrosset, T. W. Berg, M. Van Der Poel, J. Mørk, and B. Tromborg, J. Phys. D. Appl. Phys. **38**, 2088 (2005).

[2] J. P. Reithmaier, G. Eisenstein, and A. Forchel, Proc. IEEE **95**, 1779 (2007).

[3] Ł. Dusanowski, M. Syperek, P. Mrowiński, W. Rudno-Rudziński, J. Misiewicz, A. Somers, S. Höfling, M. Kamp, J. P. Reithmaier, and G. Sęk, Appl. Phys. Lett. **105**, 021909 (2014).

[4] Ł. Dusanowski, M. Syperek, W. Rudno-Rudziński, P. Mrowiński, G. Sek, J. Misiewicz, A. Somers, J. P. Reithmaier, S. Höfling, and A. Forchel, Appl. Phys. Lett. **103**, 253113 (2013).

[5] P. Mrowiński, A. Musiał, A. Maryński, M. Syperek, J. Misiewicz, A. Somers, J. P. Reithmaier, S. Höfling, and G. Sęk, Appl. Phys. Lett. **106**, 053114 (2015).

[6] M. B. Ward, M. C. Dean, R. M. Stevenson, A. J. Bennett, D. J. P. Ellis, K. Cooper, I. Farrer, C. A. Nicoll, D. A. Ritchie, and A. J. Shields, Nat. Commun. **5**, 3316 (2014).

[7] R. M. Stevenson, R. J. Young, P. Atkinson, K. Cooper, D. A. Ritchie, and A. J. Shields, Nature **439**, 179 (2006).

[8] P. Mrowiński, K. Tarnowski, J. Olszewski, A. Somers, M. Kamp, S. Höfling, J. P. Reithmaier, W. Urbańczyk, J. Misiewicz, P. Machnikowski, and G. Sęk, Acta Phys. Pol. A **129**, 48 (2016).

[9] A. Musiał, P. Kaczmarkiewicz, G. Sęk, P. Podemski, P. Machnikowski, J. Misiewicz, S. Hein, S. Höfling, and A. Forchel, Phys. Rev. B - Condens. Matter Mater. Phys. **85**, 035314 (2012).

[10] P. Mrowiński, K. Tarnowski, J. Olszewski, A. Somers, M. Kamp, J. P. Reithmaier, W. Urbańczyk, J. Misiewicz, P. Machnikowski, and G. Sęk, J. Appl. Phys. **120**, 074303 (2016).

[11] A. Lundskog, C.-W. Hsu, K. Fredrik Karlsson, S. Amloy, D. Nilsson, U. Forsberg, P. Olof Holtz, and E. Janzén, Light Sci. Appl. **3**, e139 (2014).

[12] A. Sauerwald, T. Kümmell, G. Bacher, A. Somers, R. Schwertberger, J. P. Reithmaier, and A. Forchel, Appl. Phys. Lett. **86**, 253112 (2005).

[13] T. Mensing, L. Worschech, Y. Ling, S. Kaiser, R. Schwertberger, J. P. Reithmaier, and A. Forchel, Phys. Status Solidi C Conf. **82**, 1161 (2003).

[14] G. Sek, P. Podemski, A. Musiał, J. Misiewicz, S. Hein, S. Höfling, and A. Forchel, J. Appl. Phys. **105**, 086104 (2009).

[15] E. Waks, K. Inoue, C. Santori, D. Fattal, J. Vučković, G. S. Solomon, and Y. Yamamoto, Nature **420**, 762 (2002).

[16] E. Knill, R. Laflamme, and G. J. Milburn, Nature **409**, 46 (2001).

[17] P. Kok, W. J. Munro, K. Nemoto, T. C. Ralph, J. P. Dowling, and G. J. Milburn, Rev. Mod. Phys. **79**, 135 (2007).

[18] C. L. Salter, R. M. Stevenson, I. Farrer, C. A. Nicoll, D. A. Ritchie, and A. J. Shields, Nature **465**, 594 (2010).

[19] C. Santori, D. Fattal, J. Vučković, G. S. Solomon, and Y. Yamamoto, Nature **419**, 594 (2002).

[20] J. M. Gérard, B. Sermage, B. Gayral, B. Legrand, E. Costard, and V. Thierry-Mieg, Phys. Rev. Lett. **81**, 1110 (1998).

[21] E. Peter, P. Senellart, D. Martrou, A. Lemaître, J. Hours, J. M. Gérard, and J. Bloch, Phys. Rev. Lett. **95**, 067401 (2005).

[22] M. H. Baier, A. Malko, E. Pelucchi, D. Y. Oberli, and E. Kapon, Phys. Rev. B **73**, 205321 (2006).

[23] R. Trotta, A. Polimeni, F. Martelli, G. Pettinari, M. Capizzi, L. Felisari, S. Rubini, M. Francardi, A. Gerardino, P. C. M. Christianen, and J. C. Maan, Adv. Mater. **23**, 2706 (2011).

[24] V. Baumann, F. Stumpf, C. Schneider, S. Kremling, L. Worschech, A. Forchel, S. Höfling, and M. Kamp, Appl. Phys. Lett. **100**, 091109 (2012).

[25] L. Seravalli, C. Bocchi, G. Trevisi, and P. Frigeri, J. Appl. Phys. **108**, 114313 (2010).

[26] J. Kettler, M. Paul, F. Olbrich, K. Zeuner, M. Jetter, P. Michler, M. Florian, C. Carmesin, and F. Jahnke, Phys. Rev. B **94**, 045303 (2016).

[27] G. Saint-Girons, N. Chauvin, A. Michon, G. Patriarche, G. Beaudoin, G. Bremond, C. Bru-Chevallier, and I. Sagnes, Appl. Phys. Lett. **88**, 133101 (2006).

[28] N. Chauvin, B. Salem, G. Bremond, G. Guillot, C. Bru-Chevallier, and M. Gendry, J. Appl. Phys. **100**, 073702 (2006).

[29] N. Chauvin, E. Tranvouez, G. Bremond, G. Guillot, C. Bru-Chevallier, E. Dupuy, P. Regreny, M. Gendry, and G. Patriarche, Nanotechnology **17**, 1831 (2006).

[30] N. I. Cade, H. Gotoh, H. Kamada, H. Nakano, S. Anantathanasarn, and R. Nötzel, Appl. Phys. Lett. **89**, 181113 (2006).

[31] N. I. Cade, H. Gotoh, H. Kamada, H. Nakano, and H. Okamoto, Phys. Rev. B **73**, 115322 (2006).

[32] V. V. Belykh, A. Greilich, D. R. Yakovlev, M. Yacob, J. P. Reithmaier, M. Benyoucef, and M. Bayer, Phys. Rev. B **92**, 165307 (2015).

[33] V. Mlinar, M. Bozkurt, J. M. Ulloa, M. Ediger, G. Bester, A. Badolato, P. M. Koenraad, R. J. Warburton, and A. Zunger, Phys. Rev. B **80**, 165425 (2009).

[34] S. Rodt, A. Schliwa, K. Pötschke, F. Guffarth, and D. Bimberg, Phys. Rev. B **71**, 155325 (2005).

[35] R. Seguin, A. Schliwa, S. Rodt, K. Potschke, U. W. Pohl, and D. Bimberg, Phys. Rev. Lett. **95**, 257402 (2005).

[36] W. Langbein, P. Borri, U. Woggon, V. Stavarache, D. Reuter, and A. D. Wieck, Phys. Rev. B **70**, 033301 (2004).

[37] J. J. Finley, D. Mowbray, M. Skolnick, A. Ashmore, C. Baker, A. Monte, and M. Hopkinson, Phys. Rev. B **66**, 153316 (2002).

[38] C. Jarlov, P. Gallo, M. Calic, B. Dwir, A. Rudra, and E. Kapon, Appl. Phys. Lett. **101**, 191101 (2012).

[39] A. Schliwa, M. Winkelnkemper, and D. Bimberg, Phys. Rev. B **79**, 075443 (2009).

[40] L. He, M. Gong, C.-F. Li, G.-C. Guo, and A. Zunger, Phys. Rev. Lett. **101**, 157405 (2008).

[41] M. Abbarchi, C. Mastrandrea, T. Kuroda, T. Mano, K. Sakoda, N. Koguchi, S. Sanguinetti, A. Vinattieri, and M. Gurioli, Phys. Rev. B **78**, 125321 (2008).

[42] M. Zieliński, Phys. Rev. B - Condens. Matter Mater. Phys. **88**, 155319 (2013).

[43] R. Singh and G. Bester, Phys. Rev. B **84**, 241402(R) (2011).

[44] M. Zieliński, Phys. Rev. B **86**, 115424 (2012).

[45] J. W. Luo and A. Zunger, Phys. Rev. B **84**, 235317 (2011).

[46] M. Zieliński, K. Gołasa, M. R. Molas, M. Goryca, T. Kazimierczuk, T. Smoleński, A. Golnik, P. Kossacki, A. A. L. Nicolet, M. Potemski, Z. R. Wasilewski, and A. Babiński, Phys. Rev. B **91**, 085303 (2015).

[47] H. Dery, E. Benisty, A. Epstein, R. Alizon, V. Mikhelashvili, G. Eisenstein, R. Schwertberger, D. Gold, J. P. Reithmaier, and A. Forchel, J. Appl. Phys. **95**, 6103 (2004).

[48] I. Vurgaftman, J. R. Meyer, and L. R. Ram-Mohan, J. Appl. Phys. **89**, 5815 (2001).

[49] K. Nishi, H. Saito, S. Sugou, and J. S. Lee, Appl. Phys. Lett. **74**, 1111 (1999).

[50] A. Somers, W. Kaiser, J. P. Reithmaier, A. Forchel, M. Gioaninni, and I. Montrosset, Appl. Phys. Lett. **89**, 061107 (2006).

[51] P. Mrowiński, A. Musiał, G. Sęk, J. Misiewicz, S. Höfling, A. Somers, S. Hein, and A. Forchel, Acta Phys. Pol. A **124**, 801 (2013).

[52] P. N. Keating, Phys. Rev. **145**, 637 (1966).

[53] R. M. Martin, Phys. Rev. B **1**, 4005 (1970).
[54] M. Zieliński, M. Korkusiński, and P. Hawrylak, Phys. Rev. B **81**, 085301 (2010).
[55] G. Sęk, K. Ryczko, M. Motyka, J. Andrzejewski, K. Wysocka, J. Misiewicz, L. H. Li, A. Fiore, and G. Patriarche, J. Appl. Phys. **101**, 063539 (2007).
[56] J.-M. Jancu, R. Scholz, F. Beltram, and F. Bassani, Phys. Rev. B **57**, 6493 (1998).
[57] M. Zieliński, J. Phys. Condens. Matter **25**, 465301 (2013).
[58] M. Zieliński, Nanoscale Res. Lett. **7**, 265 (2012).
[59] G. A. Narvaez, G. Bester, and A. Zunger, Phys. Rev. B - Condens. Matter Mater. Phys. **72**, 245318 (2005).
[60] P. Machnikowski, Phys. Rev. B - Condens. Matter Mater. Phys. **83**, 1 (2011).
[61] M. Bayer, G. Ortner, O. Stern, A. Kuther, A. Gorbunov, A. Forchel, P. Hawrylak, S. Fafard, K. Hinzer, T. Reinecke, S. N. Walck, J. P. Reithmaier, F. Klopf, and F. Schäfer, Phys. Rev. B **65**, 195315 (2002).
[62] R. Singh and G. Bester, Phys. Rev. B **88**, 075430 (2013).
[63] M. A. Dupertuis, K. F. Karlsson, D. Y. Oberli, E. Pelucchi, A. Rudra, P. O. Holtz, and E. Kapon, Phys. Rev. Lett. **107**, 127403 (2011).
[64] K. F. Karlsson, M. A. Dupertuis, D. Y. Oberli, E. Pelucchi, A. Rudra, P. O. Holtz, and E. Kapon, Phys. Rev. B **81**, 161307 (2010).
[65] J. H. Versluis, A. V. Kimel, A. Kirilyuk, P. Grabs, F. Lehmann, G. Schmidt, L. W. Molenkamp, and Th. Rasing, Phys. Rev. B **80**, 193303 (2009).